International Journal of Fatigue 30 (2008) 2175–2190

Contents lists available at ScienceDirect

International Journal of Fatigue

journal homepage: www.elsevier.com/locate/ijfatigue

Fatigue behavior of aluminum 5754-O and 6111-T4 spot friction welds in lap-shear specimens

V.-X. Tran [a], J. Pan [a,*], T. Pan [b]

[a] Mechanical Engineering, University of Michigan, Ann Arbor, MI 48109, USA
[b] Ford Research and Advanced Engineering, Ford Motor Company, Dearborn, MI 48131, USA

ARTICLE INFO

Article history:
Received 2 December 2007
Received in revised form 20 May 2008
Accepted 23 May 2008
Available online 13 June 2008

Keywords:
Spot friction weld
Friction stir spot weld
Failure mode
Fatigue life
Kinked crack
Structural stress

ABSTRACT

Fatigue behavior of aluminum 5754-O and 6111-T4 spot friction welds in lap-shear specimens is investigated based on experimental observations and two fatigue life estimation models. Optical micrographs of the 5754 and 6111 welds made by a concave tool and a flat tool, respectively, before and after failure under quasi-static and cyclic loading conditions are examined. The micrographs show that the failure modes of the 5754 and 6111 welds under quasi-static and cyclic loading conditions are quite different. Under quasi-static loading conditions, both types of welds mainly fail from the nearly flat fracture surface through the nugget. Under low-cycle loading conditions, both types of welds mainly fail from the kinked crack through the upper sheet thickness and the fracture surface through the nugget. Under high-cycle loading conditions, both types of welds mainly fail from the kinked cracks through the upper and lower sheet thicknesses. A kinked fatigue crack growth model based on the stress intensity factor solutions for finite kinked cracks and a structural stress model based on the closed-form structural stress solutions at the critical locations of the welds are adopted to estimate the fatigue lives of both types of welds. The fatigue life estimations based on the kinked fatigue crack growth model and the structural stress model appear to agree well with the experimental results for both types of welds.

1. Introduction

Resistance spot welding is the most commonly used joining technique for body-in-white parts made of steel sheets. However, resistance spot welding of aluminum sheets is likely to produce poor welds as reported by Thornton et al. [1] and Gean et al. [2]. Recently, a spot friction welding technology for joining aluminum sheets has been developed by Mazda Motor Corporation and Kawasaki Heavy Industry [3,4]. The most significant advantage of the spot friction welding process comparing to the conventional welding processes is that the joint can be made without melting the base metal. A schematic illustration of the spot friction welding process was presented, for example, in Lin et al. [5].

The mechanical behavior of aluminum spot friction welds under quasi-static loading conditions was studied, for example, see Lin et al. [5], Pan et al. [6], Fujimoto et al. [7,8] and Hinrichs et al. [9]. The metallurgical aspects of aluminum 6111 spot friction welds were investigated by Mitlin et al. [10]. Tran et al. [11] investigated the failure loads of spot friction welds in aluminum 6111 lap-shear specimens under quasi-static and dynamic loading conditions. Recently, Lin et al. [12–15] investigated the fatigue behavior of spot friction welds made by different tools in aluminum 6111 sheets based on experimental observations and fracture mechanics. A comprehensive literature review for spot friction welds can be found in Pan [16]. Note that most of the literature is for spot friction welds between similar aluminum sheets. However, dissimilar spot friction welds between aluminum 2017-T6 and 5052 sheets, between aluminum 5754 and 6111 sheets, and between aluminum 5754-O and 7075-T6 sheets were investigated by Tozaki et al. [17], Su et al. [18] and Tran et al. [19], respectively.

It should be noted that aluminum 5754 alloys are widely employed in the automotive industry to produce parts such as internal door stiffeners or the entire body-in-white as reported in Kaufman [20]. However, the fatigue behavior of aluminum 5754 spot friction welds has not been extensively studied. In this paper, we investigate the fatigue behavior of aluminum 5754 and 6111 spot friction welds in lap-shear specimens based on experimental observations and two fatigue life estimation models. Optical micrographs of the welds before and after failure under quasi-static and cyclic loading conditions are examined to investigate the fracture and failure mechanisms of both types of welds. Based on the experimental observations of the paths of the dominant kinked fatigue cracks, the kinked fatigue crack growth model as discussed in Lin et al. [12–15] with the global stress intensity factor solutions for the main cracks obtained from three-dimensional finite element analyses is adopted to estimate the fatigue lives of the welds. The structural stress model based on the closed-form structural

* Corresponding author. Tel.: +1 734 764 9404; fax: +1 734 647 3180.
E-mail address: jwo@umich.edu (J. Pan).

0142-1123/$ - see front matter © 2008 Elsevier Ltd. All rights reserved.
doi:10.1016/j.ijfatigue.2008.05.025

stress solutions at the critical locations of the spot welds as reported in Lin and Pan [21] and the experimental stress-life fatigue data is also adopted to estimate the fatigue lives of the welds. Finally, the estimated fatigue lives based on the kinked fatigue crack growth model and the structural stress model are compared with the experimental results for both types of welds.

2. 5754 and 6111 spot friction welds before testing

For the spot friction welding process under load-controlled conditions, the important welding processing parameters are the tool geometry, the tool rotational speed, the tool downward force and the processing time. In this investigation, a tool with a concave shoulder and a threaded probe pin was used to make spot friction welds in lap-shear specimens of aluminum 5754-O sheets of the thickness of 2.0 mm. A tool rotational speed of 3000 rpm and a tool downward force of 5.88 kN were specified to make the 5754 spot friction welds. The 5754 welds were first made at different processing times and tested under lap-shear loading conditions. The optimal processing time for the maximum failure strength of the 5754 welds in lap-shear specimens under this particular set of the welding processing parameters was identified. This optimal processing time and the welding processing parameters specified above were then used to make the 5754 spot friction welds tested in this investigation.

In this investigation, another tool with a flat shoulder was used to make spot friction welds in lap-shear specimens of aluminum 6111-T4 sheets. For the 6111 welds, the thicknesses of the upper and lower sheets are 0.94 mm and 1.04 mm, respectively. The 6111 welds tested in this investigation were made based on a DOE (design of experiments) method to determine the optimal tool rotational speed, tool downward force and processing time for the maximum failure strength of the 6111 welds in lap-shear specimens. Note that the 6111 lap-shear specimens used in this investigation and those used in Tran et al. [11] are identical. The 6111 lap-shear specimens used in this investigation were made of the upper and lower sheets of unequal thicknesses while the 6111 lap-shear specimens used in Lin et al. [13,15] were made of the upper and lower sheets of equal thickness. We first present some optical and scanning electron micrographs of the cross sections along the symmetry planes of the 5754 and 6111 spot friction welds before testing.

Fig. 1a shows an optical micrograph of the cross section along the symmetry plane of a 5754 spot friction weld made by the concave tool before testing. As shown in the figure, the indentation profile reflects the general shape of the threaded probe pin and the concave shoulder of the tool. The bottom surface of the lower sheet is almost flat. The area near the central hole represents the fine grain stir zone where the upper and lower sheets are well bonded possibly due to high pressure and large plastic deformation. Two notches, marked as N1 and N2, can be seen in the figure. Fig. 1b shows a close-up optical micrograph of region I in Fig. 1a, where the notch, marked as N2, extends and becomes a crack. The location of the crack tip is marked in the figure. Fig. 1c shows a close-up optical micrograph of region II in Fig. 1b. As shown in Fig. 1c, the interfacial surface between the two deformed sheet materials materials near the crack tip slightly rises up outside the stir zone. The location of the crack tip is also marked in the figure. The location of the crack tip can be identified by a scanning electron micrograph of the crack tip region as shown in Fig. 1d. As shown in the figure, some part of the crack surface near the tip becomes vague and may be bonded by the welding process.

As shown in Fig. 1a, the thickness of the weld nugget near the central hole is slightly larger than that near the outer circumference of the tool shoulder indentation due to the concave geometry of the tool shoulder. The concave tool shoulder squeezed out some upper sheet material but maintained some upper sheet material near the central hole. As suggested in Fig. 1a, the material under the tool shoulder indentation flowed outward and resulted in a radial expansion of the upper sheet material along the outer circumference of the tool shoulder indentation. However, due to the constraint of the neighboring material, the upper sheet was therefore slightly bent along the outer circumference of the tool shoulder indentation.

Fig. 2a shows an optical micrograph of the cross section along the symmetry plane of a 6111 spot friction weld made by the flat tool before testing. As shown in the figure, the indentation profile reflects the shape of the probe pin and the flat shoulder of the tool. The bottom surface of the lower sheet is almost flat. The area near the central hole represents the fine grain stir zone where the upper and lower sheets are well bonded possibly due to high pressure and large plastic deformation. Two notches, marked as N1 and N2, can be seen in the figure. Fig. 2b shows a close-up optical micrograph of region I in Fig. 2a, where the notch, marked as N2, extends and becomes a crack. The location of the crack tip is marked in the figure. Fig. 2c shows a close-up optical micrograph of region II in Fig. 2b where the interfacial surface, marked by two small arrows, becomes vague and disappears into the stir zone. As shown in Fig. 2c, the interfacial surface between the two deformed sheet materials near the crack tip remained almost planar outside the stir zone. The location of the crack tip is also marked in the figure. The location of the crack tip can also be identified by a scanning electron micrograph of the crack tip region as shown in Fig. 2d. As shown in the figure, some part of the crack surface near the tip becomes vague and may be bonded by the welding process.

As shown in Fig. 2a, the flat tool shoulder squeezed out a portion of the upper sheet material and, consequently, the thickness of the upper sheet decreased under the shoulder indentation. As suggested in Fig. 2a, the material under the tool shoulder indentation flowed outward and resulted in a radial expansion of the upper sheet material along the outer circumference of the shoulder indentation. However, due to the constraint of the neighboring material, the upper sheet was therefore slightly bent along the outer circumference of the tool shoulder indentation.

3. Experiments

The lap-shear specimens were made by using two 25.4 mm by 101.6 mm aluminum sheets with a 25.4 mm by 25.4 mm overlap area. Figs. 3a and b show a 5754 lap-shear specimen with a spot friction weld made by the concave tool and a 6111 lap-shear specimen with a spot friction weld made by the flat tool, respectively. As shown in Fig. 3a, two square doublers of 25.4 mm $\times$ 25.4 mm made of aluminum 5754 sheets are attached to the ends of the 5754 lap-shear specimen. As shown in Fig. 3b, two doublers are made by folding two square parts of the sheets near the ends (25.4 mm $\times$ 25.4 mm) of the 6111 lap-shear specimen. Note that the doublers are used to align the applied load to avoid the initial realignment of the specimen under lap-shear loading conditions and to reinforce the sheet materials near the holes. Due to the load-controlled welding process, the actual plunge depths of the tool penetration and the geometries of the spot friction welds may not be controlled precisely under the same welding processing parameters. In order to minimize the effects of the weld geometry on the experimental results, we selected the specimens with the spot friction welds that have nearly the same actual plunge depths of the tool penetration for the quasi-static and fatigue tests. Before testing, all 6111 specimens were baked in an oven at 170 °C for 20 minutes and cooled in the ambient air to simulate the paint bake cycles in automotive assembly plants.

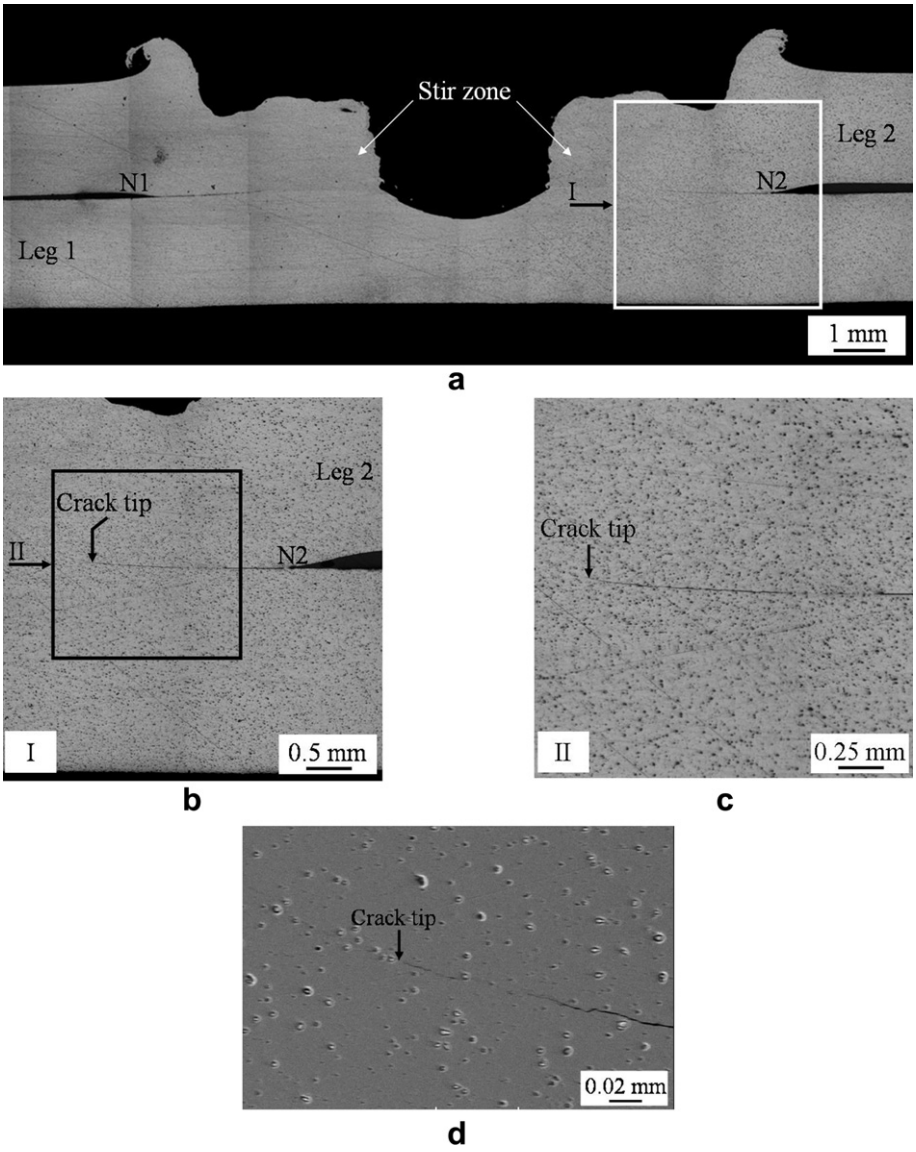

Fig. 1. (a) An optical micrograph of the cross section along the symmetry plane of a 5754 spot friction weld made by the concave tool before testing, (b) a close-up optical micrograph of region I, (c) a close-up optical micrograph of region II, (d) a close-up scanning electron micrograph of the crack tip region as shown in (c).

Lap-shear specimens were first tested under quasi-static loading conditions by using an Instron testing machine at a monotonic displacement rate of 1.0 mm per minute. The load and displacement were simultaneously recorded during each test. The average failure loads, defined as the maximum loads of the load–displacement curves, obtained from three tested 5754 and 6111 lap-shear specimens are 4.34 kN and 3.38 kN, respectively. These failure loads were used as the reference loads to determine the loads applied in the fatigue tests. The lap-shear specimens were then tested under cyclic loading conditions by using an Instron servo-hydraulic fatigue testing machine with the load ratio R of 0.2. The test frequency was 10 Hz. The tests were terminated when specimens were separated, or nearly separated when the displacement of the two grips of specimens exceeded 5 mm. Some tests were stopped before the final failures of the specimens to examine the fatigue crack growth patterns. Fig. 3c shows the experimental results for the 5754 spot friction welds made by the concave tool and the 6111 spot friction welds made by the flat tool in lap-shear specimens under cyclic loading conditions. The number of specimens available for fatigue testing is limited.

4. Failure modes of 5754 welds under quasi-static and cyclic loading conditions

4.1. A two-dimensional overview of failure modes

We conducted experiments for the 5754 spot friction welds in lap-shear specimens under quasi-static and cyclic loading conditions. Based on the experimental observations, the failed 5754 spot friction welds under quasi-static loading conditions show one failure mode. The failed 5754 spot friction welds under cyclic loading conditions with the fatigue lives from 10^3 cycles to 10^4 cycles (low-cycle fatigue) show a different failure mode. The failed 5754 spot friction welds under cyclic loading conditions with the fatigue lives from 10^4 cycles to 2×10^5 cycles (high-cycle fatigue) show another failure mode. Note that we define low-cycle fatigue and high-cycle fatigue loading conditions only for convenient presentation in this paper. The fatigue life and the load range for the transition of the failure mode from low-cycle fatigue to high-cycle fatigue for the 5754 spot friction welds are about 1.46×10^4 cycles and 2.01 kN, respectively, as shown in Fig. 3c. Since the failure modes of the

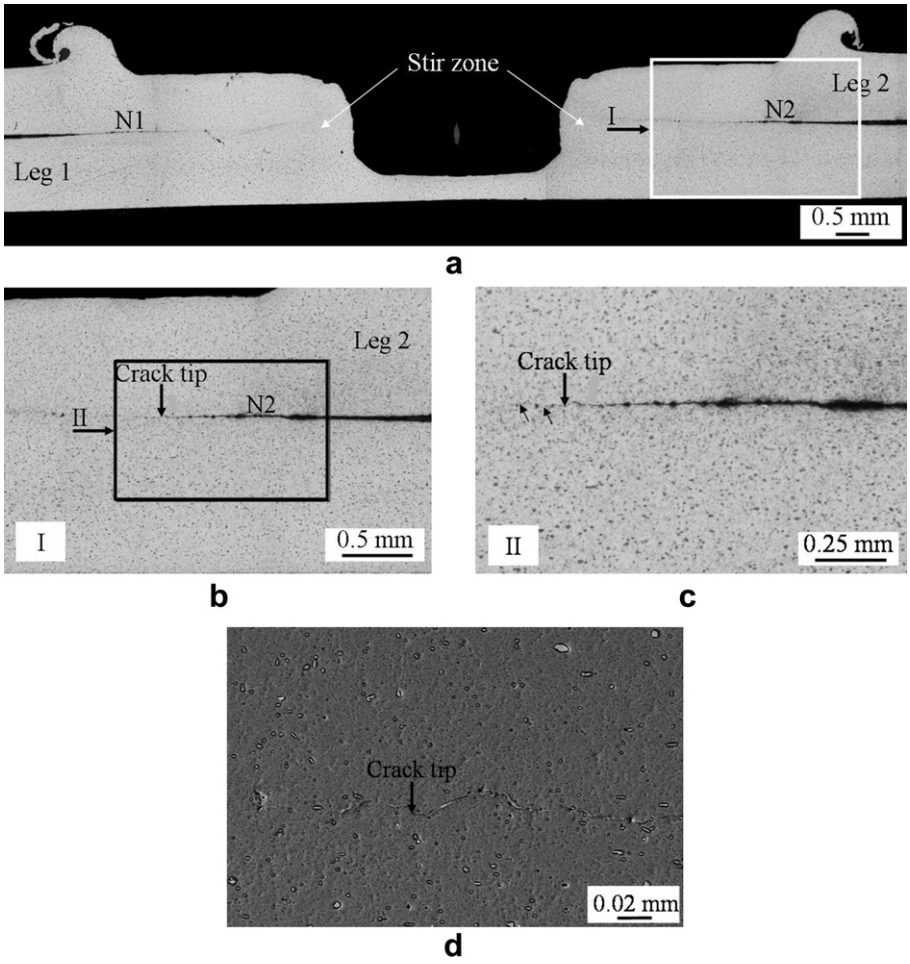

Fig. 2. (a) An optical micrograph of the cross section along the symmetry plane of a 6111 spot friction weld made by the flat tool before testing, (b) a close-up optical micrograph of region I, (c) a close-up optical micrograph of region II, (d) a close-up scanning electron micrograph of the crack tip region as shown in (c).

5754 spot friction welds are quite complex under quasi-static and cyclic loading conditions, we first present a two-dimensional general overview of the failure modes under quasi-static, low-cycle and high-cycle loading conditions.

Fig. 4a shows a schematic plot of a 5754 lap-shear specimen made by the concave tool with the sheet thickness $t = 2$ mm under an applied resultant shear load (shown as the bold arrows). Fig. 4b shows a schematic plot of the cross section along the symmetry plane of the 5754 spot friction weld made by the concave tool. In this figure, the short dash lines near the two notches represent the unwelded interfacial surfaces and the thin solid lines represent either the fracture surfaces or fatigue cracks. Fig. 4c summarizes the failure modes of the 5754 spot friction welds in lap-shear specimens under quasi-static, low-cycle and high-cycle loading conditions.

As shown in Fig. 4b and as summarized in Fig. 4c, under quasi-static loading conditions, cracks A and B appear to emanate from the original crack tips of the weld. Crack A propagates upward a bit possibly along the interfacial surface and then into the upper sheet thickness while crack B propagates a bit along the interfacial surface. When the load continues to increase, the upper and lower sheets are eventually separated by fracture surfaces C and D. Under low-cycle loading conditions, fatigue cracks B and E appear to emanate from the original crack tips of the weld and propagate upward a bit possibly along the interfacial surface and through the upper sheet thickness, respectively. A shear failure, marked by F, occurs at the end of fatigue crack E. Then, the failure propagates along the nugget circumference. Near the final stage of the specimen failure, crack B becomes crack G that propagates partially into the lower sheet thickness. Eventually, the stir zone is separated by fracture surfaces H and D. Finally, the upper sheet is torn off.

Under high-cycle loading conditions, fatigue cracks E and I appear to emanate from the original crack tips of the weld and propagate through the upper and lower sheet thicknesses, respectively. A shear failure, marked by F, occurs at the end of fatigue crack E. Under high-cycle loading conditions with higher load ranges, after propagating through the upper and lower sheet thicknesses, fatigue crack E becomes a circumferential crack that propagates along the nugget circumference while fatigue crack I becomes a transverse through crack that propagates in the width direction of the specimen. These two cracks finally cause the failure of the specimen. Under high-cycle loading conditions with lower load ranges, after propagating through the upper and lower sheet thicknesses, both fatigue cracks E and I become transverse through cracks that propagate in the width direction of the specimen. These two cracks finally cause the failure of the specimen.

As shown in Fig. 1a, the interfacial surface between the two deformed sheet materials of the 5754 spot friction weld in the stir zone can hardly be seen. Note that the welding processing parameters used to make the 5754 welds tested in this investigation are nearly the same as those used to make the dissimilar 5754/7075 welds at the optimal processing time tested in Tran et al. [19]. Note also that the upper aluminum 5754 sheets used in this investigation and in Tran et al. [19] are identical. Therefore, the geometry

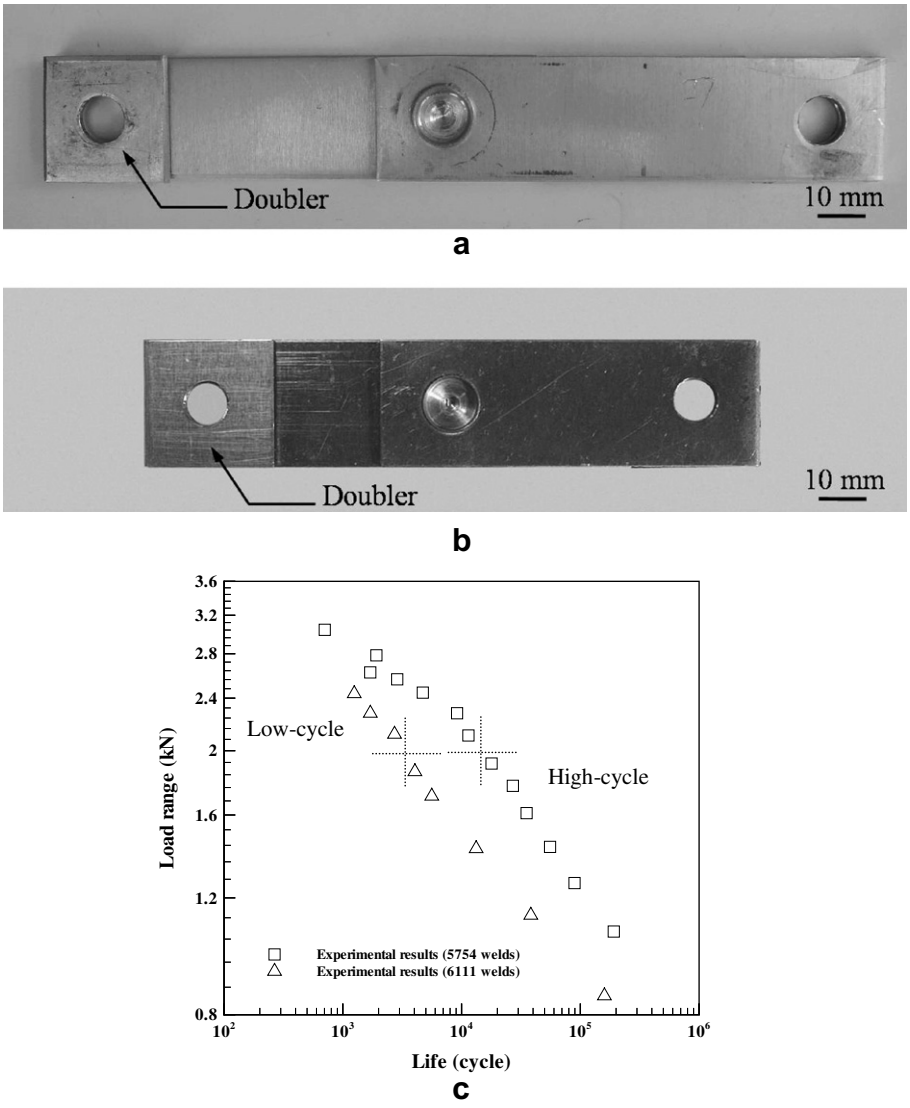

Fig. 3. (a) A 5754 lap-shear specimen with a spot friction weld made by the concave tool, (b) a 6111 lap-shear specimen with a spot friction weld made by the flat tool, (c) experimental results for the 5754 spot friction welds made by the concave tool and the 6111 spot friction welds made by the flat tool in lap-shear specimens under cyclic loading conditions.

of the interfacial surface between the two deformed sheet materials of the 5754 welds tested in this investigation may be similar to that of the dissimilar 5754/7075 welds at the optimal processing time as shown in Tran et al. [19]. According to Tran et al. [19], the lower sheet material of the dissimilar 5754/7075 welds at the optimal processing time rises and extends significantly into the upper sheet material near the central hole. Therefore, it seems that fracture or crack surfaces C, D, G and H in Fig. 4b may not separate along the interfacial surface between the two deformed sheet materials of the 5754 welds. In the following, we present the micrographs to show the details of the failure modes of the 5754 welds in lap-shear specimens under different loading conditions.

4.2. Failure mode under quasi-static loading conditions

Fig. 5 shows an optical micrograph of the cross section along the symmetry plane of a failed 5754 spot friction weld made by the concave tool in a lap-shear specimen under quasi-static loading conditions. The bold arrows in Fig. 5 schematically show the direction of the applied load. Due to the large deformation in the final stage of the specimen failure, the nugget rotated clockwise. Therefore, the sheets near the nugget are slightly bent. The loads are marked schematically parallel to the legs of the specimens as shown. The applied load stretches the upper right sheet (marked as Leg 2) and the lower left sheet (marked as Leg 1). As shown in Fig. 5, two cracks, marked as crack 1 and crack 2, appear to emanate from the original crack tips of the weld. Crack 1 propagates a bit along the interfacial surface while crack 2 propagates upward a bit possibly along the interfacial surface (see Fig. 1) and then into the upper sheet thickness due to the favorable stress condition. When the load continues to increase, the upper and lower sheets are eventually separated by the nearly flat fracture surface through the nugget, marked as S1 and S2, in Fig. 5. In summary, the 5754 welds mainly fail from the nearly flat fracture surface through the nugget under quasi-static loading conditions.

4.3. Failure mode under low-cycle loading conditions

Figs. 6a and b show optical micrographs of the cross sections along the symmetry planes of a partially failed 5754 spot friction weld made by the concave tool at the fatigue life of 3.5×10^3 cycles and a failed 5754 spot friction weld made by the concave tool at

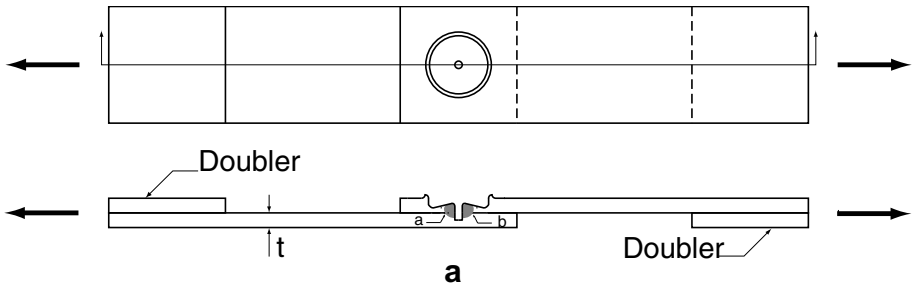

a

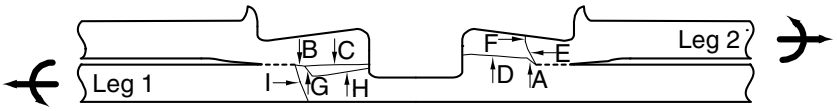

b

		Failure mode
Quasi-static		A, B → C, D
Low-cycle		E → F → Circumferential crack B → G → H, D
High-cycle	Higher load ranges	E → F → Circumferential crack I → Transverse through crack
	Lower load ranges	E → F → Transverse through crack I → Transverse through crack

c

Fig. 4. (a) A schematic plot of a 5754 lap-shear specimen made by the concave tool with the sheet thickness $t = 2$ mm under an applied resultant shear load (shown as the bold arrows), (b) a schematic plot of the cross section along the symmetry plane of the 5754 spot friction weld made by the concave tool, (c) failure modes of the 5754 spot friction welds in lap-shear specimens under quasi-static, low-cycle and high-cycle loading conditions.

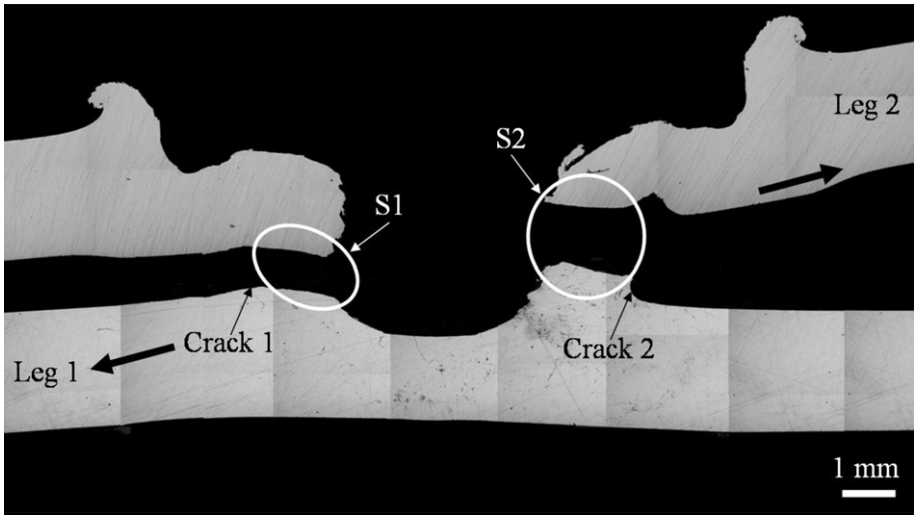

Fig. 5. An optical micrograph of the cross section along the symmetry plane of a failed 5754 spot friction weld made by the concave tool in a lap-shear specimen under quasi-static loading conditions.

the fatigue life of 4.7×10^3 cycles under a load range of 2.45 kN, respectively. Note that the lap-shear specimen with the partially failed spot friction weld was subjected to the same load range as the lap-shear specimen with the failed spot friction weld. However, we stopped the test for the partially failed spot friction weld at about 75% of the fatigue life of the failed spot friction weld under the same load range to examine the fatigue crack growth pattern before the final failure. Therefore, the spot friction weld in Fig. 6a, marked with $0.75N_f$, was partially failed and not separated while the spot friction weld in Fig. 6b, marked with N_f, was failed and separated. We will follow the same notation for other figures presented later in the paper. The bold arrows in Figs. 6a and b schematically show the direction of the applied load. Near the lower left portions of the welds, fatigue cracks, marked as crack 1 in Figs. 6a and b, appear to emanate from the original crack tips and propagate upward a bit possibly along the interfacial surface (see Fig. 1). Near the upper right portions of the welds, fatigue cracks, marked as crack 2 in Figs. 6a and b, appear to emanate from the original crack tips and propagate upward a bit possibly along the interfacial surface and then into the upper sheet thickness due to

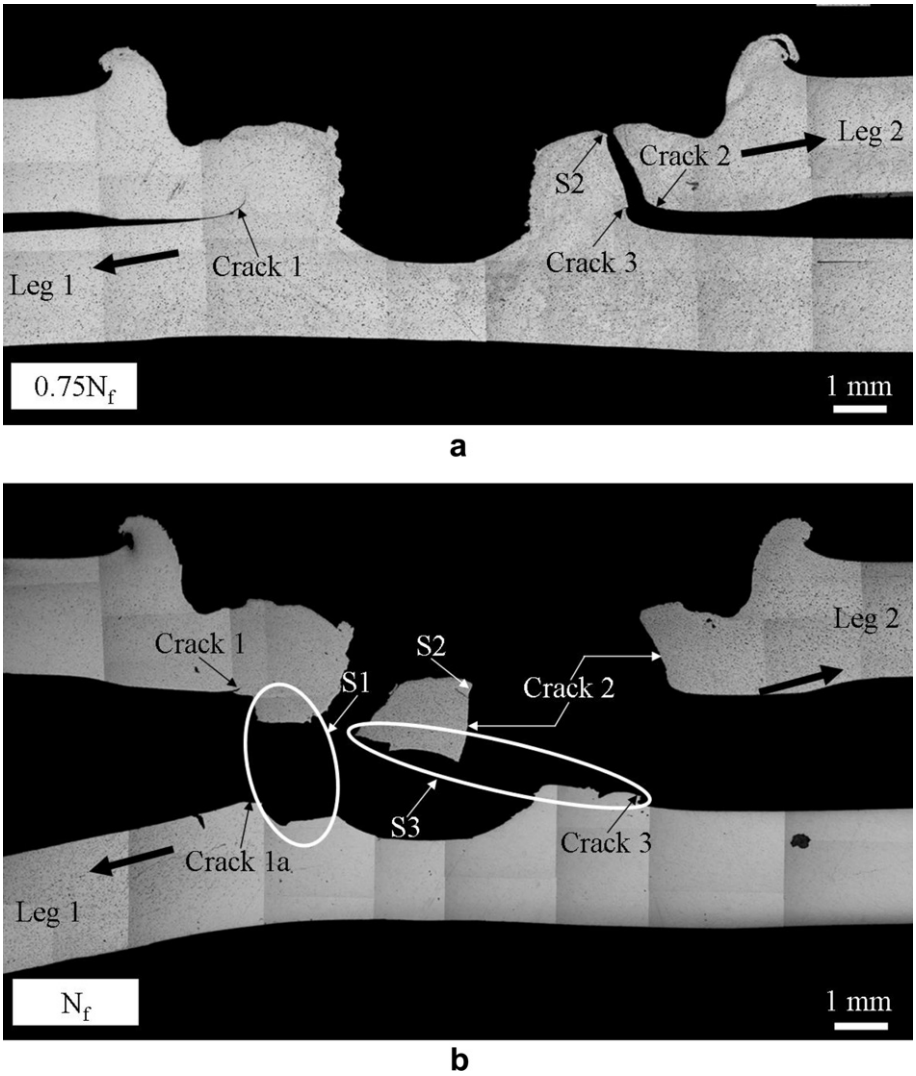

Fig. 6. Optical micrographs of the cross sections along the symmetry planes of (a) a partially failed 5754 spot friction weld made by the concave tool at the fatigue life of 3.5×10^3 cycles and (b) a failed 5754 spot friction weld made by the concave tool at the fatigue life of 4.7×10^3 cycles under a load range of 2.45 kN.

the favorable stress condition. As shown in Fig. 6a, another small crack, marked as crack 3, appears to be initiated near the fatigue life of 3.5×10^3 cycles. As shown in Figs. 6a and b, a shear failure, marked by S2, occurs at the end of fatigue crack 2. The failure then propagates along the nugget circumference. After fatigue crack 2 propagates through the upper sheet thickness and around the nugget circumference, without the support of the upper sheet near the stretching side of the nugget, the nugget is rotated clockwise and the sheets near the nugget are therefore bent. As shown in Fig. 6b, crack 1 does not grow but the original crack becomes crack 1a that propagates downward into the lower sheet thickness and then through the nugget near the final stage of the specimen failure. Eventually, the stir zone is separated first by a fracture surface through the left portion of the nugget marked as S1 due to crack 1a as shown in Fig. 6b and then by a fracture surface through the right portion of the nugget marked as S3 due to crack 3 as shown in Fig. 6b. The upper sheet is finally torn off. As shown in Figs. 6a and b, fatigue crack 2 can be considered as a kinked crack emanating from the original crack tip on the right side of the weld. As suggested in Figs. 6a and b, fatigue crack 2 appears to be the dominant kinked fatigue crack that causes the failure of the 5754 welds under low-cycle loading conditions. In summary, the 5754 welds mainly fail from the kinked crack through the upper sheet thickness and the nearly flat fracture surface through the nugget under low-cycle loading conditions.

4.4. Failure mode under high-cycle loading conditions

Figs. 7a and b show optical micrographs of the cross sections along the symmetry planes of a partially failed 5754 spot friction weld made by the concave tool at the fatigue life of 4.2×10^4 cycles and a failed 5754 spot friction weld made by the concave tool at the fatigue life of 5.5×10^4 cycles under a load range of 1.43 kN, respectively. Note that the spot friction welds in Figs. 7a and b were not separated. The bold arrows in Figs. 7a and b schematically show the direction of the applied load. In Figs. 7a and b, two fatigue cracks, marked as crack 1′ and crack 2′ in each of the figures, appear to emanate from the original crack tips of the welds and propagate into the lower and upper sheet thicknesses, respectively. As shown in Fig. 7a, fatigue crack 1′ propagates partially into the lower sheet thickness while fatigue crack 2′ propagates through the upper sheet thickness (with a reduced thickness). Note that the length of fatigue crack 1′ is smaller than that of fatigue crack 2′ at the fatigue life of 4.2×10^4 cycles as indicated in Fig. 7a. As shown in Fig. 7b, both fatigue cracks 1′ and 2′ propagate through the lower and upper sheet thicknesses, respectively. A shear

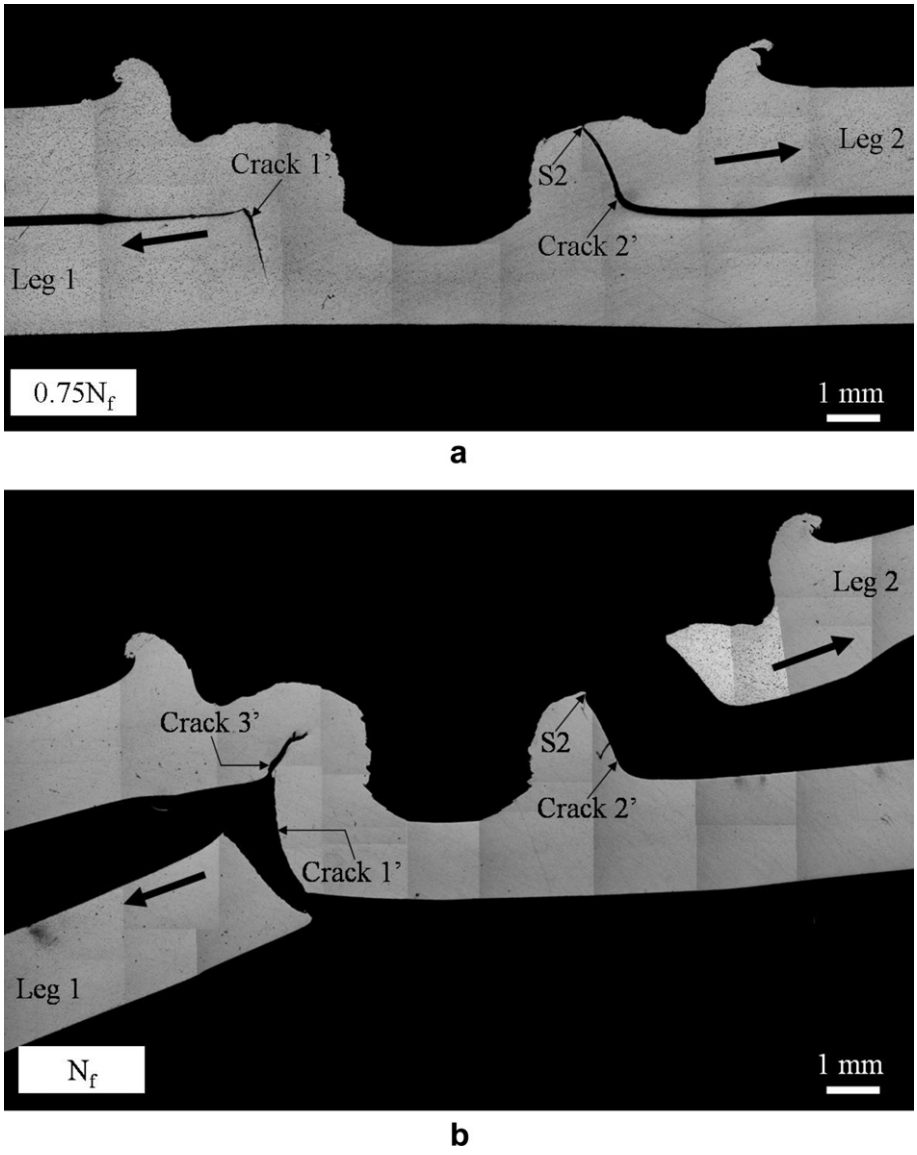

Fig. 7. Optical micrographs of the cross sections along the symmetry planes of (a) a partially failed 5754 spot friction weld made by the concave tool at the fatigue life of 4.2×10^4 cycles and (b) a failed 5754 spot friction weld made by the concave tool at the fatigue life of 5.5×10^4 cycles under a load range of 1.43 kN.

failure, marked by S2, occurs at the end of fatigue crack 2′ as shown in Figs. 7a and b. Note that another crack, marked as crack 3′ in Fig. 7b, was likely formed during the welding process or introduced at the cross-sectional cutting of the failed specimen since no similar crack was found in the partially failed specimen as shown in Fig. 7a. Note also that this crack should not affect the fatigue behavior of the 5754 welds since the crack is subjected to an unfavorable stress condition for crack propagation.

Under high-cycle loading conditions with higher load ranges, after propagating through the lower and upper sheet thicknesses, fatigue crack 1′ becomes a transverse through crack that propagates in the width direction of the specimen while fatigue crack 2′ becomes a circumferential crack that propagates along the nugget circumference. These two cracks finally cause the failure of the specimen. Under high-cycle loading conditions with lower load ranges, after propagating through the lower and upper sheet thicknesses, both fatigue cracks 1′ and 2′ become transverse through cracks that propagate in the width direction of the specimen. These two cracks finally cause the failure of the specimen. As shown in Figs. 7a and b, both fatigue cracks 1′ and 2′ can be considered as kinked cracks emanating from the original crack tips of the welds. As suggested in Figs. 7a and b, fatigue crack 2′ appears to be the dominant kinked fatigue crack that causes the failure of the 5754 welds under high-cycle loading conditions. In summary, the 5754 welds mainly fail from the kinked cracks through the upper and lower sheet thicknesses under high-cycle loading conditions.

5. Failure modes of 6111 welds under quasi-static and cyclic loading conditions

5.1. A two-dimensional overview of failure modes

We conducted experiments for the 6111 spot friction welds in lap-shear specimens under quasi-static and cyclic loading conditions. Based on the experimental observations, the failed 6111 spot friction welds under quasi-static loading conditions show one failure mode. The failed 6111 spot friction welds under cyclic loading conditions with the fatigue lives from 10^3 cycles to 3×10^3 cycles (low-cycle fatigue) show a different failure mode. The failed 6111 spot friction welds under cyclic loading conditions with the fatigue lives from 3×10^3 cycles to 1.6×10^5 cycles (high-cycle fatigue) show another failure mode. Note that we define low-cycle fatigue

and high-cycle fatigue loading conditions only for convenient presentation in this paper. The fatigue life and the load range for the transition of the failure mode from low-cycle fatigue to high-cycle fatigue for the 6111 spot friction welds are about 3×10^3 cycles and 1.99 kN, respectively, as shown in Fig. 3c. Since the failure modes of the 6111 spot friction welds are quite complex under quasi-static and cyclic loading conditions, we first present a two-dimensional general overview of the failure modes under quasi-static, low-cycle and high-cycle loading conditions.

Fig. 8a shows a schematic plot of a 6111 lap-shear specimen made by the flat tool with the upper sheet thickness $t = 0.94$ mm and the lower sheet thickness $t' = 1.04$ mm under an applied resultant shear load (shown as the bold arrows). Fig. 8b shows a schematic plot of the cross section along the symmetry plane of the 6111 spot friction weld made by the flat tool. In this figure, the short dash lines near the two notches represent the unwelded interfacial surfaces and the thin solid lines represent either the fracture surfaces or fatigue cracks. Fig. 8c summarizes the failure modes of the 6111 welds in lap-shear specimens under quasi-static, low-cycle and high-cycle loading conditions.

In general, the failure modes of the 6111 welds made by the flat tool in lap-shear specimens under quasi-static and cyclic loading conditions as shown in Fig. 8b and as summarized in Fig. 8c are similar to those of the 5754 welds made by the concave tool in lap-shear specimens as discussed earlier. Under quasi-static loading conditions, cracks A′ and B′ appear to emanate from the original crack tips of the weld and propagate upward a bit into the upper sheet thickness and a bit along the interfacial surface, respectively. When the load continues to increase, the upper and lower sheets are eventually separated by fracture surfaces B′ and C′. Under low-cycle loading conditions, fatigue cracks D′ and F′ appear to emanate from the original crack tips of the weld and propagate through the upper sheet thickness and partially into the lower sheet thickness, respectively. A shear failure, marked by E′, occurs at the end of fatigue crack D′. The failure then propagates along the nugget circumference. After fatigue crack D′ propagates through the upper sheet thickness and along the nugget circumference, the stir zone is eventually separated by fracture surface B′. Finally, the upper sheet is torn off.

Under high-cycle loading conditions, fatigue cracks D′ and F′ appear to emanate from the original crack tips of the weld and propagate into the upper and lower sheet thicknesses, respectively. Under high-cycle loading conditions with higher load ranges, after propagating through the upper and lower sheet thicknesses, both fatigue cracks D′ and F′ become circumferential cracks that propagate along the nugget circumference. The upper sheet is finally torn off. Under high-cycle loading conditions with lower load ranges, after propagating through the upper and lower sheet thicknesses, both fatigue cracks D′ and F′ become transverse through cracks that propagate in the width direction of the specimen. These two cracks finally cause the failure of the specimen.

As shown in Fig. 2a, the interfacial surface between the two deformed sheet materials of the 6111 spot friction weld in the stir zone can hardly be seen. Note that Fig. 2 in Lin et al. [15] shows a deformed shape of a 6111 spot friction weld made by a flat tool based on an axisymmetric thermal–mechanical finite element modeling of the spot friction welding process. As shown in the figure, the lower sheet material is pushed upward near the central hole. Therefore, it seems that fracture surfaces B′ and C′ in Fig. 8b may not separate along the interfacial surface between the two deformed sheet materials of the 6111 spot friction welds tested in this investigation. In the following, we present the micrographs to show the details of the failure modes of the 6111 spot friction welds in lap-shear specimens under different loading conditions.

5.2. Failure mode under quasi-static loading conditions

Fig. 9 shows an optical micrograph of the cross section along the symmetry plane of a failed 6111 spot friction weld made by the flat tool in a lap-shear specimen under quasi-static loading conditions.

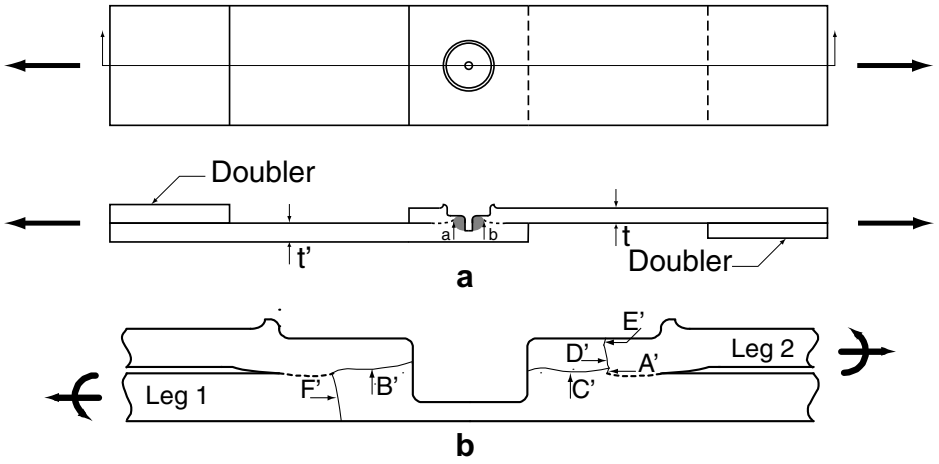

		Failure mode
Quasi-static		A', B' → C'
Low-cycle		D' → E' → Circumferential crack F' → B'
High-cycle	Higher load ranges	D', F' → Circumferential cracks
	Lower load ranges	D', F' → Transverse through cracks

c

Fig. 8. (a) A schematic plot of a 6111 lap-shear specimen made by the flat tool with the upper sheet thickness of $t = 0.94$ mm and the lower sheet thickness $t' = 1.04$ mm under an applied resultant shear load (shown as the bold arrows), (b) a schematic plot of the cross section along the symmetry plane of the 6111 spot friction weld made by the flat tool, (c) failure modes of the 6111 spot friction welds in lap-shear specimens under quasi-static, low-cycle and high-cycle loading conditions.

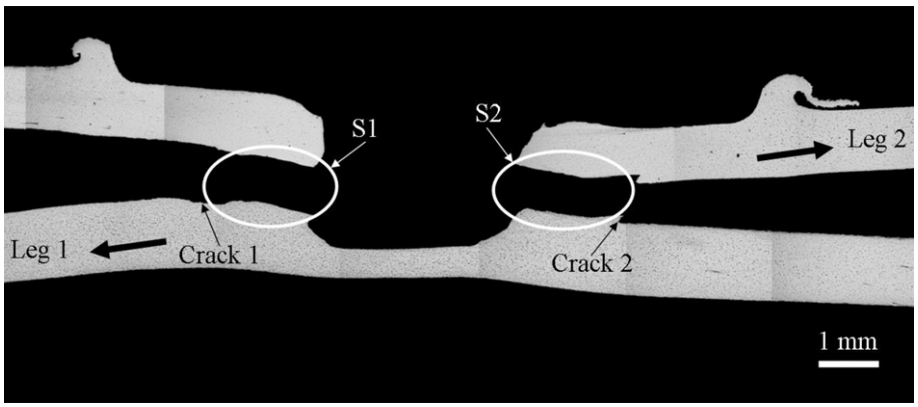

Fig. 9. An optical micrograph of the cross section along the symmetry plane of a failed 6111 spot friction weld made by the flat tool in a lap-shear specimen under quasi-static loading conditions.

The bold arrows in Fig. 9 schematically show the direction of the applied load. The applied load stretches the upper right sheet (marked as Leg 2) and the lower left sheet (marked as Leg 1). As shown in Fig. 9, two cracks, marked as crack 1 and crack 2, appear to emanate from the original crack tips of the weld. Crack 1 propagates a bit along the interfacial surface while crack 2 propagates upward a bit into the upper sheet thickness possibly due to the favorable stress condition. When the load continues to increase, the upper and lower sheets are eventually separated with the nearly flat fracture surface through the nugget, marked as S1 and S2, in Fig. 9. Similar to the 5754 welds, the 6111 welds mainly fail from the nearly flat fracture surface through the nugget under quasi-static loading conditions.

5.3. Failure mode under low-cycle loading conditions

Figs. 10a and b show optical micrographs of the cross sections along the symmetry planes of a partially failed 6111 spot friction weld made by the flat tool at the fatigue life of 2.0×10^3 cycles and a failed 6111 spot friction weld made by the flat tool at the fatigue life of 2.7×10^3 cycles under a load range of 2.13 kN, respectively. Note that the spot friction weld in Fig. 10b was separated.

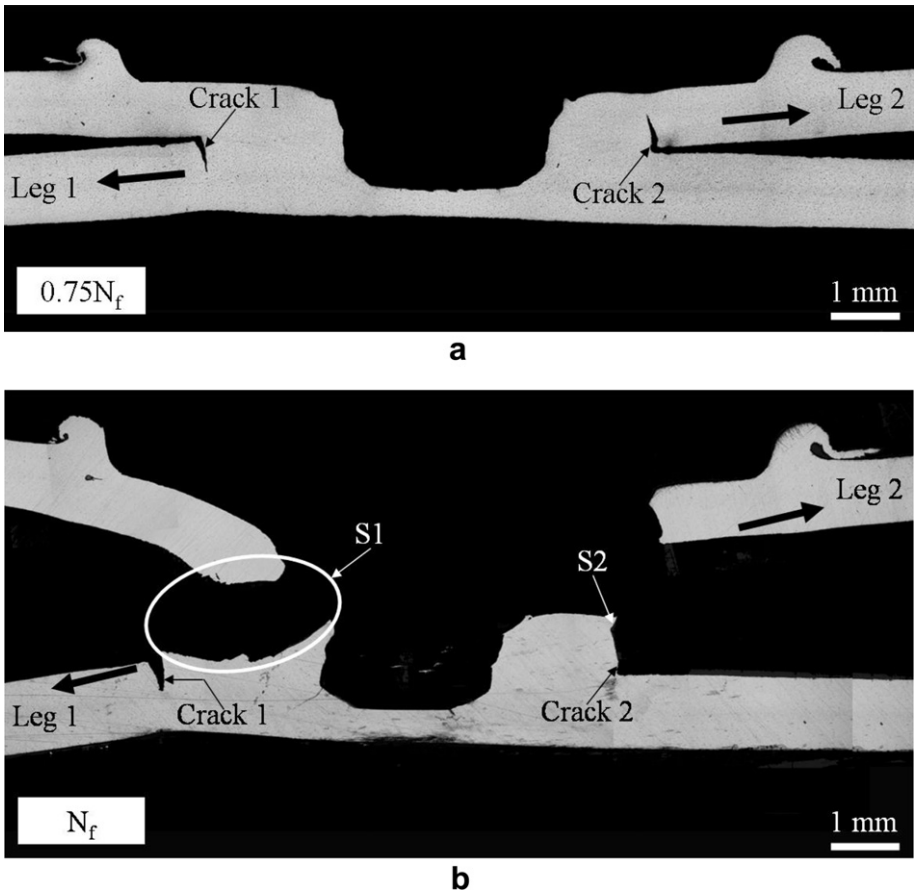

Fig. 10. Optical micrographs of the cross sections along the symmetry planes of (a) a partially failed 6111 spot friction weld made by the flat tool at the fatigue life of 2.0×10^3 cycles and (b) a failed 6111 spot friction weld made by the flat tool at the fatigue life of 2.7×10^3 cycles under a load range of 2.13 kN.

The bold arrows in Figs. 10a and b schematically show the direction of the applied load. As shown in Figs. 10a and b, two fatigue cracks, marked as crack 1 and crack 2 in each of the figures, appear to emanate from the original crack tips of the welds and propagate into the lower and upper sheet thicknesses, respectively. As shown in Fig. 10a, both fatigue cracks propagate partially into the lower and upper sheet thicknesses at the fatigue life of 2.0×10^3 cycles. Note that the lengths of both fatigue cracks are nearly the same at the fatigue life of 2.0×10^3 cycles as indicated in Fig. 10a. As shown in Fig. 10b, fatigue crack 1 propagates partially into the lower sheet thickness while fatigue crack 2 propagates through the upper sheet thickness at the fatigue life of 2.7×10^3 cycles. A shear failure, marked by S2, occurs at the end of fatigue crack 2. The failure then propagates along the nugget circumference. After fatigue crack 2 propagates through the upper sheet thickness and around the nugget circumference, without the support of the upper sheet, the nugget is rotated clockwise and the sheets near the nugget are therefore bent. Eventually, the stir zone is separated by a fracture surface through the left portion of the nugget, marked as S1, in Fig. 10b. The upper sheet is finally torn off. As shown in Figs. 10a and b, both fatigue cracks 1 and 2 can be considered as kinked cracks emanating from the original crack tips of the welds. As suggested in Figs. 10a and b, fatigue crack 2 appears to be the dominant kinked fatigue crack that causes the failure of the 6111 welds under low-cycle loading conditions. In summary, the 6111 welds mainly fail from the kinked crack through the upper sheet thickness and the fracture surface through the nugget under low-cycle loading conditions.

5.4. Failure mode under high-cycle loading conditions

Figs. 11a and b show optical micrographs of the cross sections along the symmetry planes of a partially failed 6111 spot friction weld made by the flat tool at the fatigue life of 1.2×10^5 cycles and a *failed* 6111 spot friction weld made by the flat tool at the fatigue life of 1.6×10^5 cycles under a load range of 0.85 kN, respectively. The bold arrows in Figs. 11a and b schematically show the direction of the applied load. In Figs. 11a and b, two fatigue cracks, marked as crack 1′ and crack 2′ in each of the figures, appear to emanate from the original crack tips of the welds and propagate into the lower and upper sheet thicknesses, respectively. As shown in Fig. 11a, both fatigue cracks propagate partially into the lower and upper sheet thicknesses at the fatigue life of 1.2×10^5 cycles. As shown in Fig. 11a, the length of fatigue crack 1′ is much larger than that of fatigue crack 2′ at the fatigue life of 1.2×10^5 cycles. As shown in Fig. 11b, both fatigue cracks propagate through the lower and upper sheet thicknesses at the fatigue life of 1.6×10^5 cycles. As shown in Fig. 11b, the length of fatigue crack 1′ is slightly larger than that of fatigue crack 2′ at the fatigue life of 1.6×10^5 cycles. Note that another crack, marked as crack 3′ in Fig. 11b, appears to emanate from the original crack tip on the left side of the weld and propagates first a bit along the interfacial surface and then through the left portion of the nugget. This crack appears to be initiated near the final stage of the specimen failure since no similar crack was seen in Fig. 11a.

Under high-cycle loading conditions with higher load ranges, after propagating through the lower and upper sheet thicknesses, both fatigue cracks 1′ and 2′ become circumferential cracks that propagate along the nugget circumference. Finally, the upper sheet is torn off. Under high-cycle loading conditions with lower load ranges, after propagating through the lower and upper sheet thicknesses, both fatigue cracks 1′ and 2′ become transverse through cracks that propagate in the width direction of the specimen. These two cracks finally cause the failure of the specimen. As shown in Figs. 11a and b, both fatigue cracks 1′ and 2′ can be considered as kinked cracks emanating from the original crack tips of the welds. As suggested in Figs. 11a and b, fatigue crack 1′ appears to be the dominant kinked fatigue crack that causes the failure of the 6111 welds under high-cycle loading conditions. Similarly to the 5754 welds, the 6111 welds mainly fail from the kinked cracks

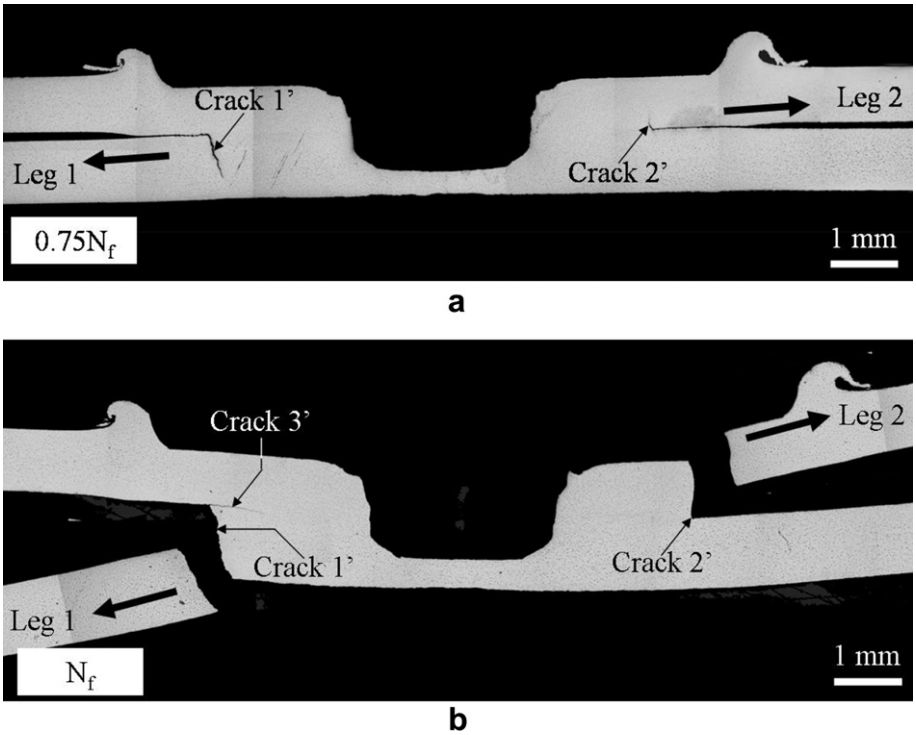

Fig. 11. Optical micrographs of the cross sections along the symmetry planes of (a) a partially failed 6111 spot friction weld made by the flat tool at the fatigue life of 1.2×10^5 cycles and (b) a failed 6111 spot friction weld made by the flat tool at the fatigue life of 1.6×10^5 cycles under a load range of 0.85 kN.

through the upper and lower sheet thicknesses under high-cycle loading conditions.

6. Fatigue life estimation models

In order to develop engineering fatigue life estimation models, we idealize the three-dimensional spot friction weld problem as a two-dimensional crack problem as in Newman and Dowling [22] and Lin et al. [23]. Figs. 12a and b show schematic plots of the cross sections along the symmetry planes of the 5754 and 6111 spot friction welds, respectively, under a statically equivalent combined tensile and bending load shown as the bold arrows in the figures. In Figs. 12a and b, the short dash lines near the notches represent the unwelded interfacial surfaces and the thin solid lines represent the fatigue cracks. According to Lin et al. [14,15,23,24], the global stress intensity factors solutions K_I and K_{II} are maximum at the original crack tips on the cross section along the symmetry plane of the spot weld in lap-shear specimens. These critical locations are marked as *a* and *b* in Figs. 12a and b (and also in Figs. 4a and 8a).

6.1. A kinked fatigue crack growth model

As discussed earlier, the fatigue crack growth behaviors of the 5754 spot friction welds made by the concave tool under low-cycle and high-cycle loading conditions are quite similar, whereas the final failure modes of the welds under loading conditions of low-cycle fatigue and high-cycle fatigue are different, as shown in Figs. 6 and 7. As schematically shown in Fig. 12a, two kinked fatigue cracks, marked as kinked crack 1 and kinked crack 2, are initiated from the original crack tips of the weld with the kink angles α_1 and α_2, respectively. Based on the experimental observations, the failures of the 5754 spot friction welds made by the concave tool under cyclic loading conditions appear to be dominated by kinked crack 2 that propagates through the upper sheet thickness (with a reduced thickness). Note that the kink angle α_2 of kinked crack 2 is estimated from Figs. 6 and 7 to be 69° for the 5754 welds under cyclic loading conditions.

As discussed earlier, the fatigue crack growth behavior and the final failure mode of 6111 spot friction welds made by the flat tool under low-cycle loading conditions are quite similar to those under high-cycle loading conditions as shown in Figs. 10 and 11. As schematically shown in Fig. 12b, two kinked fatigue cracks, marked as kinked crack 1 and kinked crack 2, are initiated from the original crack tips of the weld with the kink angles α_1 and α_2, respectively. Based on the experimental observations, the failure of the 6111 welds made by the flat tool under low-cycle loading conditions appears to be dominated by kinked crack 2 that propagates through the upper sheet thickness (with a reduced thickness). Note that the kink angle α_2 of kinked crack 2 is estimated to be 75° from Fig. 10 for the 6111 welds under low-cycle loading conditions. However, the failure of the 6111 welds made by the flat tool under high-cycle loading conditions appears to be dominated by kinked crack 1 that propagates through the lower sheet thickness. Note that the kink angle α_1 of kinked crack 1 is estimated to be 75° from Fig. 11 for the 6111 welds under high-cycle loading conditions.

Here, we adopt the kinked fatigue crack growth model with consideration of the local stress intensity factor solutions for finite kinked cracks as discussed in details in Lin et al. [12–15]. It should be emphasized that the theoretical solutions for the global stress intensity factors K_I and K_{II} for the main cracks used in Lin et al. [12–15] are based on the works of Lin et al. [23] and Zhang [25] for resistance spot welds in lap-shear specimens, respectively. Due to the complex geometries of the 5754 and 6111 spot friction welds, three-dimensional finite element analyses based on the micrographs of the cross sections along the symmetry planes of the 5754 and 6111 spot friction welds shown in Figs. 1a and 2a, respectively, were employed to obtain the accurate global stress intensity factors along the crack front of the weld nuggets. The global stress intensity factors K_I and K_{II} solutions at the critical locations obtained from the finite element analyses are then used to estimate the fatigue lives of both types of spot friction welds. The local stress intensity factor solutions k_I and k_{II} for the finite kinked cracks in this investigation are determined as in Lin et al. [12–15] with consideration of the finite kink length.

6.2. A structural stress model

Radaj [26] and Radaj and Zhang [27–29] established the foundation to use the structural stresses to determine the stress intensity factors for spot welds under various types of loading conditions. Zhang [25,30] presented closed-form stress intensity factor solutions at the critical locations of spot welds in various types of specimens based on the analytical stress solutions for a plate with a rigid inclusion under various types of loading conditions, and correlated the solutions with the experimental results. It should be emphasized that the authors mentioned above used the structural stresses to estimate the stress intensity factor solutions at the critical locations of spot welds to correlate with the experimental results under cyclic loading conditions. In the following, we present a structural stress model based on the closed-form structural stress solutions at the critical locations of the welds and the experimental

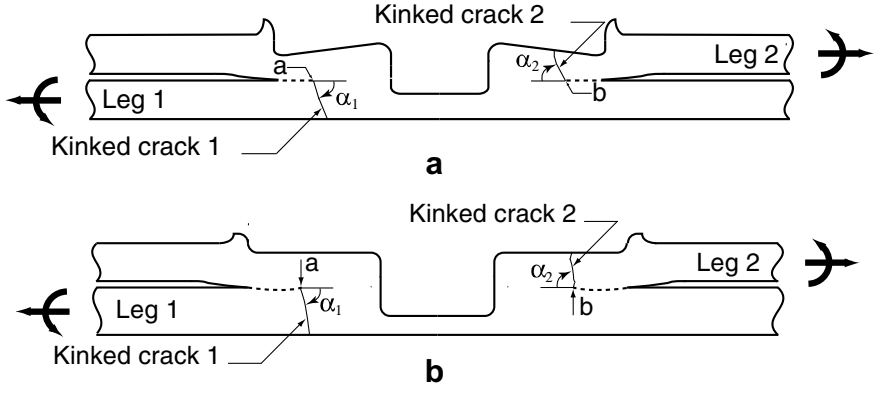

Fig. 12. (a) A schematic plot of the cross section along the symmetry plane of the 5754 spot friction weld under a statically equivalent combined tensile and bending load (shown as the bold arrows), (b) a schematic plot of the cross section along the symmetry plane of the 6111 spot friction weld under a statically equivalent combined tensile and bending load (shown as the bold arrows).

stress-life fatigue data to estimate the fatigue lives of the spot friction welds in lap-shear specimens.

Lin and Pan [21] recently derived closed-form structural stress solutions for spot welds under lap-shear loading conditions based on the stress function approach and the Kirchoff plate theory for linear elastic materials. The closed-form structural stress solutions for spot welds under lap-shear loading conditions were developed from the analytical closed-form stress solutions for a plate with a rigid inclusion subjected to a resultant shear load. This resultant shear load was decomposed into four types of symmetric and anti-symmetric loads of counter bending, central bending, in-plane shear and tension. The total structural stress σ_{total} at the critical locations of a spot weld in a lap-shear specimen under a resultant shear load F is presented here as a function of the radius a of the spot weld (idealized as a rigid inclusion), the relevant sheet thickness t, the half width b of the lap-shear specimen and the Poisson's ratio v as

$$\sigma_{\text{total}} = \frac{-3F}{8btXY}[2b^2X + 4Y(a^4b^4 + b^8)] + \frac{3F}{2\pi at} + \frac{F}{2\pi at} + \frac{F}{4bt}\left[\frac{1}{1+v} - \frac{2}{v-3}\right] \quad (1)$$

where X and Y are defined as

$$X = (-1+v)(a^4+b^4)^2 - 4a^2b^6(1+v) \quad (2)$$

$$Y = a^2(-1+v) - b^2(1+v) \quad (3)$$

Note that the four terms on the right hand side of Eq. (1) correspond to the structural stresses at the critical locations for a finite plate with a rigid inclusion under counter bending, central bending, in-plane shear and tension loading conditions, respectively. Note also that Lin and Pan [21] idealized the spot weld nugget as a rigid inclusion and assumed that the inclusion is perfectly bonded to the neighboring plate material in their theoretical models to derive Eq. (1). Note that the geometries of the spot friction welds shown in Figs. 1a and 2a are slightly different but in general similar to those of resistance spot welds. Note also that the material strength of the stir zone in the weld nugget of the spot friction weld should be much larger than that of the base material due to the small grain size as reported in Lin et al. [5]. As discussed earlier, the dominant kinked fatigue cracks were initiated at the critical locations a and b. Therefore, Eq. (1) can be adopted to estimate the structural stress range at the critical locations a and b of the spot friction welds for a given load range. By using Eq. (1) for the structural stress range at the critical locations a and b for the two-dimensional crack model and the experimental stress-life fatigue data of the aluminum 5754-O and 6111-T4 sheets, we can estimate the fatigue lives of the 5754 and 6111 spot friction welds in lap-shear specimens, respectively.

7. Fatigue life estimations

As discussed in Lin et al. [12–15], the spot weld radius a, the relevant sheet thickness t, the half width b of the lap-shear specimen, the Poisson's ratio v and the kinked angle α are used to determine the global and local stress intensity factor solutions for the dominant kinked fatigue crack, and the material constants C and m in the Paris law are needed to estimate the fatigue lives of the spot friction welds in lap-shear specimens based on the kinked fatigue crack growth model. However, due to the complex geometries of the 5754 and 6111 spot friction welds, three-dimensional finite element analyses are used to determine the global stress intensity factors K_{I} and K_{II} solutions at the critical locations of the welds. As indicated in Eq. (1), the spot weld radius a, the relevant sheet thickness t, the half width b of the lap-shear specimen, the Poisson's ratio v and the stress-life fatigue data are needed to estimate the fatigue lives of the spot friction welds in lap-shear specimens based on the structural stress model. It should be emphasized that the relevant sheet thickness t is the thickness of the sheet through which the dominant kinked fatigue crack propagates.

Fig. 13a shows the experimental results and fatigue life estimations based on the kinked fatigue crack growth model and the structural stress model for the 5754 spot friction welds made by the concave tool in lap-shear specimens. The fatigue life estimations shown in Fig. 13a were obtained from the reduced thickness of the upper sheet $t = 1.75$ mm under the tool shoulder indentation, the weld nugget radius $a = 3.6$ mm based on the micrograph shown in Fig. 1a, the half width $b = 12.7$ mm of the lap-shear specimen and Poisson's ratio $v = 0.31$. For the kinked fatigue crack growth model, the kink angle $\alpha_2 = 69°$, estimated from the micrographs shown in Figs. 6 and 7, was used to estimate the fatigue lives of the 5754 welds. Since the material constants for the Paris law for aluminum 5754-O sheets are not available, the material constants $C = 2.0244 \times 10^{-9} \frac{\text{mm/cycle}}{(\text{MPa}\sqrt{\text{m}})^m}$ and $m = 4.64$ for aluminum

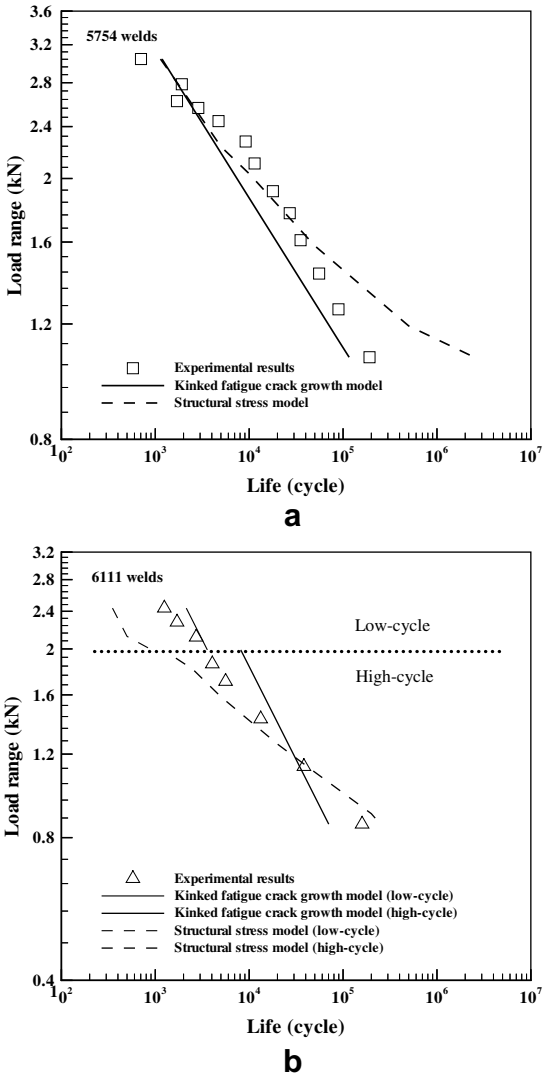

Fig. 13. (a) Experimental results and fatigue life estimations for the 5754 spot friction welds made by the concave tool in lap-shear specimens, (b) experimental results and fatigue life estimations for the 6111 spot friction welds made by the flat tool in lap-shear specimens. The symbols represent the experimental results. The solid and dash lines represent the fatigue life estimations based on the kinked fatigue crack growth model and the structural stress model, respectively.

5083-O sheets, determined from Fig. 5.24 in Campbell et al. [31], were used to estimate the fatigue lives of the 5754 welds. For the structural stress model, the experimental stress-life fatigue data of aluminum 5754-O sheets supplied by Friedman [32] were used. As shown in Fig. 13a, the estimated fatigue lives of the 5754 spot friction welds in lap-shear specimens based on the kinked fatigue crack growth model and the structural stress model agree well with the experimental results.

Fig. 13b shows the experimental results and fatigue life estimations based on the kinked fatigue crack growth model and the structural stress model for the 6111 spot friction welds made by the flat tool in lap-shear specimens. The fatigue life estimations shown in Fig. 13b were obtained from the weld nugget radius $a = 3.35$ mm based on the micrograph shown in Fig. 2a, the half width $b = 12.7$ mm of the lap-shear specimen and the Poisson's ratio $\nu = 0.31$. For the 6111 welds, the dominant kinked fatigue crack propagates through the upper sheet thickness (with a reduced thickness) under low-cycle loading conditions and through the lower sheet thickness under high-cycle loading conditions as discussed earlier. The reduced thickness of the upper sheet of $t = 0.85$ mm under the tool shoulder indentation and the thickness of the lower sheet $t = 1.04$ mm were therefore used as the relevant sheet thickness t in both fatigue life estimation models for the 6111 welds under low-cycle and high-cycle loading conditions, respectively. For the kinked fatigue crack growth model, the kink angles $\alpha_2 = \alpha_1 = 75^\circ$, estimated from the micrographs shown in Figs. 10 and 11, for the 6111 welds under low-cycle and high-cycle loading conditions, respectively, were used to estimate the fatigue lives of the 6111 welds. Since the material constants for the Paris law for aluminum 6111-T4 sheets are not available, the material constants $C = 1.35 \times 10^{-7}$ $\frac{\text{mm/cycle}}{(\text{MPa}\sqrt{\text{m}})^m}$ and $m = 2.55$ for aluminum 6014-T4 sheets [33] were used to estimate the fatigue lives of the 6111 spot friction welds as in Lin et al. [12–15]. For the structural stress model, the experimental stress-life fatigue data of baked aluminum 6111-T4 sheets supplied by Friedman [32] were used. It should be noted that the fatigue life estimations in Fig. 13b are plotted as thin lines and thick lines that correspond to the estimated fatigue lives of the 6111 welds under low-cycle and high-cycle loading conditions, respectively, due to the different values of the relevant sheet thickness t. Note that the load range for the transition of the failure mode from low-cycle fatigue to high-cycle fatigue is about 1.99 kN as shown in Figs. 3c and 13b. As shown in Fig. 13b the estimated fatigue lives of the 6111 spot friction welds based on the kinked fatigue crack growth model and the structural stress model agree well with the experimental results.

8. Discussions

Fig. 14 shows an optical micrograph of the cross section along the symmetry plane of a partially failed 5754 spot friction weld made by the concave tool under a load range of 3.38 kN at the fatigue life of 3.6×10^2 cycles which is 90% of the fatigue life of 4.0×10^2 cycles of another failed weld under the same load range. Note that this spot friction weld was not separated. It should be noted that the specimen with this partially failed weld was tested under the applied load range with a maximum load of 4.225 kN, which is about 97% of the average failure load of the 5754 lap-shear specimens under quasi-static loading conditions. As shown in Fig. 14, fatigue cracks, marked as crack 1 and crack 2, appear to emanate from the original crack tips of the weld.

Two local kinked cracks, marked as crack 2a and crack 2b, appear to emanate from kinked fatigue crack 2 after fatigue crack 2 propagates partially into the upper sheet thickness. As shown in the figure, crack 2a has a tendency to propagate through the right portion of the nugget while crack 2b has a tendency to propagate into the upper sheet thickness (with a reduced thickness). Under this very high applied load range, during the final stage of the specimen failure, crack 2a can grow faster than crack 2b and the weld can be separated in the failure mode with the nearly flat fracture surface through the nugget (similar to the failure mode shown in Fig. 5), or crack 2b can grow faster than crack 2a and the weld can be separated in the failure mode with the fracture surfaces through the upper sheet thickness and the nugget (similar to the failure mode shown in Fig. 6b). Therefore, this load range and this fatigue life can be considered as the load range and the fatigue life corresponding to the transition of the failure mode from the failure mode with the nearly flat fracture surface through the nugget to the failure mode with the fracture surfaces through the upper sheet thickness and the nugget for the 5754 welds. A micrograph indicating the similar transition of the failure mode was also observed for the 6111 welds and is not discussed here. Note that the load ranges and the fatigue lives for the transitions of the failure mode from the failure mode with the fracture surfaces through the upper sheet thickness and the nugget under low-cycle loading conditions to the failure mode with the fracture surfaces through the upper and lower sheet thicknesses under high-cycle loading conditions for the 5754 and 6111 welds are presented in Fig. 3c.

It should be noted that for the kinked fatigue crack growth model, we used the global stress intensity factor solutions obtained from the finite element analyses for the 5754 and 6111 welds based on the micrographs shown in Figs. 1a and 2a, respectively. In general, finite element computations are also needed to

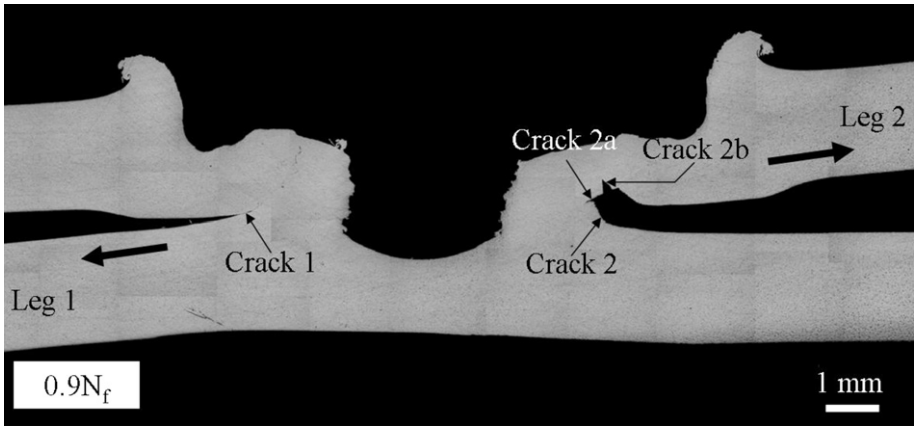

Fig. 14. An optical micrograph of the cross section along the symmetry plane of a partially failed 5754 spot friction weld made by the concave tool under a load range of 3.38 kN at the fatigue life of 3.6×10^2 cycles which is 90% of the fatigue life of 4.0×10^2 cycles of another failed weld under the same load range.

determine the accurate local stress intensity factor solutions for the kinked cracks emanating from the original crack tips of the welds with the exact weld geometries and loading conditions. However, the computational effort is quite extensive since the computations are three-dimensional in nature and the number of the cases for the weld geometries and the loading conditions are quite large. Therefore, the local stress intensity factor solutions k_{I} and k_{II} for finite kinked cracks in this investigation were determined as in Lin et al. [12–15] with consideration of the finite kink length. This model is therefore approximate in nature by considering that the geometry of the spot friction welds is different from that of the resistance spot welds. Note also that no effort is attempted to select the material constants C and m in the Paris law to fit the experimental results. Since the material constants C and m of aluminum 5754-O and 6111-T4 sheets are not available, the material constants C and m of aluminum 5083-O and 6014-T4 sheets were used to estimate the fatigue lives of the 5754 and 6111 welds, respectively. When the material constants of aluminum 5754-O and 6111-T4 sheets are available, it will be straightforward to estimate the fatigue lives of these welds.

It should be emphasized that the closed-form structural stress solutions used in the structural stress model were obtained from a linear elastic analysis. Under high-cycle loading conditions, the estimated structural stress ranges based on Eq. (1) are smaller than $2\sigma_0'$ for both types of welds where σ_0' represents the initial cyclic yield strength of the corresponding sheet materials. The cyclic behavior of materials at the critical locations a and b of the welds can be therefore considered as linear elastic under high-cycle loading conditions. Under low-cycle loading conditions, the estimated structural stress ranges based on Eq. (1) can be as high as $2.65\sigma_0'$ and $2.53\sigma_0'$ for the 5754 and 6111 welds, respectively. Neuber's type of life estimation methods can be used to improve the life estimations since the life estimations are based on the experimental stress-life fatigue data here. As shown in Figs. 13a and b, the structural stress model appears to give good estimations of the fatigue lives of both types of spot friction welds in lap-shear specimens without detailed information on the initiation and propagation of the kinked cracks emanating from the original crack tips of the welds under cyclic loading conditions. Note also that the structural stress was used to estimate the stress intensity factor solutions at the critical locations of the spot welds to correlate with the experimental results under cyclic loading conditions (Zhang [25,30]). The effects of the mean stress intensity factors on the fatigue lives of the welds may not be significant. Therefore, the mean structural stress has not been considered in the structural stress model. Further investigation is needed to fully investigate the effects of the mean stress in the structural stress model.

9. Conclusions

Fatigue behavior of aluminum 5754-O and 6111-T4 spot friction welds in lap-shear specimens is investigated based on experimental observations and two fatigue life estimation models. Optical micrographs of the 5754 and 6111 welds made by a concave tool and a flat tool, respectively, before and after failure under quasi-static and cyclic loading conditions are examined. The micrographs show that the failure modes of the 5754 and 6111 welds under quasi-static and cyclic loading conditions are quite different. Under quasi-static loading conditions, both types of welds mainly fail from the nearly flat fracture surface through the nugget. Under low-cycle loading conditions, both types of welds mainly fail from the kinked crack through the upper sheet thickness and the fracture surface through the nugget. Under high-cycle loading conditions, both types of welds mainly fail from the kinked cracks through the upper and lower sheet thicknesses. A kinked fatigue crack growth model based on the stress intensity factor solutions for finite kinked cracks and a structural stress model based on the closed-form structural stress solutions at the critical locations of the welds are adopted to estimate the fatigue lives of both types of welds. The fatigue life estimations based on the kinked fatigue crack growth model and the structural stress model appear to agree well with the experimental results for both types of welds.

Acknowledgements

The support of this work by the Ford University Research Program and the National Science Foundation under Grant No. DMI-0456755 is greatly appreciated. The support of Drs. C. Wu and C. Johnson of Ford Motor Company is greatly appreciated. The help of Mr. D. Hsu in the metallographic work is also highly appreciated.

References

[1] Thornton PH, Krause AR, Davies RG. The aluminum spot weld. Weld J 1996;75:101s–8s.
[2] Gean A, Westgate SA, Kucza JC, Ehrstrom JC. Static and fatigue behavior of spot-welded 5182-O aluminum alloy sheet. Weld J 1999;78:80s–6s.
[3] Sakano R, Murakami K, Yamashita K, Hyoe T, Fujimoto M, Inuzuka M, et al. Development of spot FSW robot system for automobile body members. In: Proceedings of the 3rd international symposium of friction stir welding, Kobe, Japan, September 27–28, 2001.
[4] Iwashita T. Method and apparatus for joining. US Patent 6601751 B2. August 5, 2003.
[5] Lin P-C, Lin S-H, Pan J, Pan T, Nicholson JM, Garman MA. Microstructures and failure modes of spot friction welds in lap-shear specimens of aluminum 6111-T4 sheets. SAE technical paper no. 2004-01-1330. Warrendale, PA: Society of Automotive Engineers; 2004.
[6] Pan T, Joaquin A, Wilkosz DE, Reatherford L, Nicholson JM. Spot friction welding for sheet aluminum joining. In: Proceedings of the 5th international symposium of friction stir welding, Metz, France, September 14–16, 2004.
[7] Fujimoto M, Inuzuka M, Nishio M, Nakashima Y. Development of friction spot joining (Report 1) – Cross sectional structures of friction spot joints. The National Meeting of Japan Welding Society, No. 74; 2004. p. 4–5.
[8] Fujimoto M, Inuzuka M, Nishio M, Nakashima Y. Development of friction spot joining (Report 2) – Mechanical properties of friction spot joints. The National Meeting of Japan Welding Society, No. 74; 2004. p. 6–7.
[9] Hinrichs JF, Smith CB, Orsini BF, DeGeorge RJ, Smale BJ, Ruehl PC. Friction stir welding for the 21st century automotive industry. In: Proceedings of the 5th international symposium of friction stir welding, Metz, France, September 14–16, 2004.
[10] Mitlin D, Radmilovic V, Pan T, Chen J, Feng Z, Santella ML. Structure–properties relations in spot friction welded (also known as friction stir spot welded) 6111 aluminum. Mater Sci Eng A 2006;441:79–96.
[11] Tran V-X, Lin P-C, Pan J, Pan T, Tyan T. Failure loads of aluminum 6111 spot friction welds under quasi-static and dynamic loading conditions. SAE technical paper no. 2007-01-0983. Warrendale, PA: Society of Automotive Engineers; 2007.
[12] Lin P-C, Pan J, Pan T. Fracture and fatigue mechanisms of spot friction welds in lap-shear specimens of aluminum 6111 sheets. SAE technical paper no. 2005-01-1247. Warrendale, PA: Society of Automotive Engineers; 2005.
[13] Lin P-C, Pan J, Pan T. Fatigue failures of aluminum 6111 spot friction welds under cyclic loading conditions. SAE technical paper no. 2006-01-1207. Warrendale, PA: Society of Automotive Engineers; 2006.
[14] Lin P-C, Pan J, Pan T. Failure modes and fatigue life estimations of spot friction welds in lap-shear specimens of aluminum 6111-T4 sheets, Part 1: Welds made by a concave tool. Int J Fatigue 2008;30:74–89.
[15] Lin P-C, Pan J, Pan T. Failure modes and fatigue life estimations of spot friction welds in lap-shear specimens of aluminum 6111-T4 sheets, Part 2: Welds made by a flat tool. Int J Fatigue 2008;30:90–105.
[16] Pan T. Friction stir spot welding (FSSW) – A literature review. SAE technical paper no. 2007-01-1702. Warrendale, PA: Society of Automotive Engineers; 2007.
[17] Tozaki Y, Uematsu Y, Tokaji K. Effect of processing parameters on static strength of dissimilar friction stir spot welds between different aluminum alloys. Fatigue Fract Eng Mater Struct 2007;30:143–8.
[18] Su P, Gerlich A, North TH, Bendzsak GJ. Intermixing in dissimilar friction stir spot welds. Metall Mater Trans A 2007;38A:584–95.
[19] Tran V-X, Pan J, Pan T. Effects of processing time on strengths and failure modes of dissimilar spot friction welds between aluminum 5754-O and 7075-T6 sheets. SAE technical paper no. 2008-01-1138. Warrendale, PA: Society of Automotive Engineers; 2008.
[20] Kaufman J-G. Introduction to aluminum alloys and tempers. Materials Park, OH: The Materials Information Society – ASM International; 2000.

[21] Lin P-C, Pan J. Closed-form structural stresses and stress intensity factor solutions for spot welds in commonly used specimens. Eng Fract Mech, submitted for publication.
[22] Newman JA, Dowling NE. A crack growth approach to life estimation of spot-welded lap joints. Fatigue Fract Eng Mater Struct 1998;21:1123–32.
[23] Lin S-H, Pan J, Wung P, Chiang J. A fatigue crack growth model for spot welds in various types of specimens under cyclic loading conditions. Int J Fatigue 2006;28:792–803.
[24] Lin P-C, Wang D-A, Pan J. Mode I stress intensity factor solutions for spot welds in lap-shear specimens. Int J Solids Struct 2007;44:1013–37.
[25] Zhang S. Stress intensities at spot welds. Int J Fract 1997;88:167–85.
[26] Radaj D. Stress singularity, notch stress and structural stress at spot-welded joints. Eng Fract Mech 1989;34:495–506.
[27] Radaj D, Zhang S. Stress intensity factors for spot welds between plates of unequal thickness. Eng Fract Mech 1991;39:391–413.
[28] Radaj D, Zhang S. Simplified formulae for stress intensity factors of spot welds. Eng Fract Mech 1991;40:233–6.
[29] Radaj D, Zhang S. Stress intensity factors for spot welds between plates of dissimilar materials. Eng Fract Mech 1992;42:407–26.
[30] Zhang S. Fracture mechanics solutions to spot welds. Int J Fract 2001;112:247–74.
[31] Campbell EJ, Gerberich WW, Underwood JH. Application of fracture mechanics for selection of metallic structural materials. Metals Parks, OH: American Society for Metals; 1982.
[32] Friedman P. Private communication; 2007.
[33] Bergner F, Zouhar G. A new approach to the correlation between the coefficient and the exponent in the power law equation of fatigue crack growth. Int J Fatigue 2000;22:229–39.